Proceedings World Geothermal Congress 2015
Melbourne, Australia, 19-25 April 2015

Geologic Modeling Workflow for Volcanic Hosted Geothermal Reservoirs: Case Study from Salak Geothermal Field

Nur Vita Aprilina[1], Drestanta Yudha Satya[1], Sri Rejeki[1], Glenn Golla[1] and Michael Waite [2]

[1] Chevron Geothermal Indonesia, Sentral Senayan II, Jalan Asia Afrika 8 Jakarta, Indonesia

[2] Chevron Energy Technology Company, 1500 Louisiana Street, Houston, Texas, USA

nvaprilina@chevron.com, drestanta@chevron.com, srejeki@chevron.com, glenn.golla@chevron.com, MWWA@chevron.com

Keywords: Salak, geothermal, reservoir, geologic model

ABSTRACT

The 3D Geologic Model is a tool for better understanding the subsurface geology and is an essential component of numerical reservoir modeling. The first Salak 3D Earth Model was built in 2005. Since then, one of the main uses of the 3D Geologic Model has been in planning and designing make-up wells. A major update of the Salak 3D Geologic Model was started in 2012 with the main objective of incorporating results of the wells drilled during the 2008-2009 and 2012-2013 drilling campaigns and about seven years of additional reservoir monitoring.

One of the challenges of geothermal reservoir modeling is the description in three dimensions of the geologic characteristics of the complex fractured systems. Volcanic geothermal reservoirs are characterized by extreme heterogeneity in lithology both laterally and vertically. Lava flows and pyroclastics are usually not deposited as widespread as sediments. Even more, in the reservoir section, lithologies can be difficult to identify from cuttings since mud and rock cuttings are often not circulated up to the surface to be sampled and examined. Due to the limited spatial distribution of deep well data, it is not an easy task to accurately estimate the distribution of reservoir and rock properties between wells. Furthermore, these subsurface heterogeneities and uncertainties influence reservoir assessment and production.

This paper documents the philosophical approach and workflows that were used to update the Salak 3D Geologic Model. Quite different from approaches taken in past geologic modeling exercises, where the limits of the "commercial" reservoir are defined in each well and then extrapolated beyond well control to build a 3D representation of the reservoir container, the Salak 3D Geologic Modeling Team emphasized the 3D description of the overall geothermal system first, thus providing a means of modeling uncertainty of the commercial limits of the reservoir directly from the 3D geocellular model.

The very first step in building the Salak 3D geologic model was to create a well–organized database of core measurements, cuttings description and wireline logs. For the rock-type modeling, lithology types described from the analysis of rock cuttings were grouped on the basis of depositional style and mineral composition to simplify the description of the heterogeneity to a level that can be justified with reasonable confidence. A stratigraphic/structural framework was created based on well correlation and surface geology outcrop description. Rock-type proportions on each stratigraphic unit were assigned based on statistics derived from the database. Another key step in modeling the Salak geothermal system was to build a detailed 3D description of pre-production (equilibrium conditions) reservoir temperatures. Hard data used to constrain the temperature model were measured well temperatures and locations of the surface thermal manifestations. Microseismicity data were used, along with temperature data, to posit the zone of thermal upwelling. Recorded occurrence of high-temperature epidote, the first permeable entry locations in the wells, integrated with resistivity from magnetotelluric survey data and interpretations help to establish the depth of the clay-altered cap, which is a key parameter for defining limits of commerciality. Porosity and permeability were assigned on the basis of formation, rock-type and depth.

The next step in the development of the Salak 3D Earth Model is define probabilistic low (P10), mid (P50) and high (P90) reservoir containers based on a number of criteria defining commerciality. Upscaling can then be performed on the gridded geologic model to produce coarser reservoir models suitable for numerical simulation.

1. INTRODUCTION

The Gunung Salak area was explored and developed for commercial power production by Union Oil of California (Unocal Geothermal Indonesia; UGI), and has been managed by Chevron Geothermal Salak since August 2005 when Chevron acquired Unocal. In February 1982, UGI entered into a Joint Operation Contract with the Indonesian National Oil Company (Pertamina) for exploration and development of the geothermal resources of the Gunung Salak Contract Area, and an Energy Sales Contract with Pertamina and the Indonesian National Power Company (PLN) for sale of steam to PLN. The contracts allowed UGI to supply steam for up to 495 MWe of electric power generation (Stimac et al., 1997).

Commercial power generation at Salak began in 1994 with a 110 MWe plant consisting of 2 x 55 MWe Units 1 and 2 operated by PLN (Murray et al., 1995). Production was expanded to 330 MWe in 1998 when 55 MWe Unit 3 (also operated by PLN) was installed adjacent to Units 1 and 2, and 3 x 55 MWe Units 4, 5 and 6 were constructed at a new location adjacent to the Awi 1 Pad (Soeparjadi et al., 1998). In 2002, generation was increased to 377 MWe as part of a new pricing agreement with the government.

As part of the reservoir management and to maintain full steam supply, make-up drilling campaigns were conducted in 2002, 2004, 2006-2007, 2008-2009 and 2012-2013. As of 2013, 107 wells had been drilled, with 82 wells being used for production and 25

wells for injection. The static (aka geologic) model was updated with new information derived from the latest drilled wells, most recent geoscientific interpretations and field performance data.

2. GEOLOGICAL FRAMEWORK

The Salak (aka Awibengkok) geothermal field is located in West Java, Indonesia along the Sunda Volcanic Arc (**Figure 1**). It is situated in a mountainous area with elevation ranging from about 950 to 1,500 m above sea level (ASL). The field is about 60 kilometers from Jakarta, capital city of Indonesia.

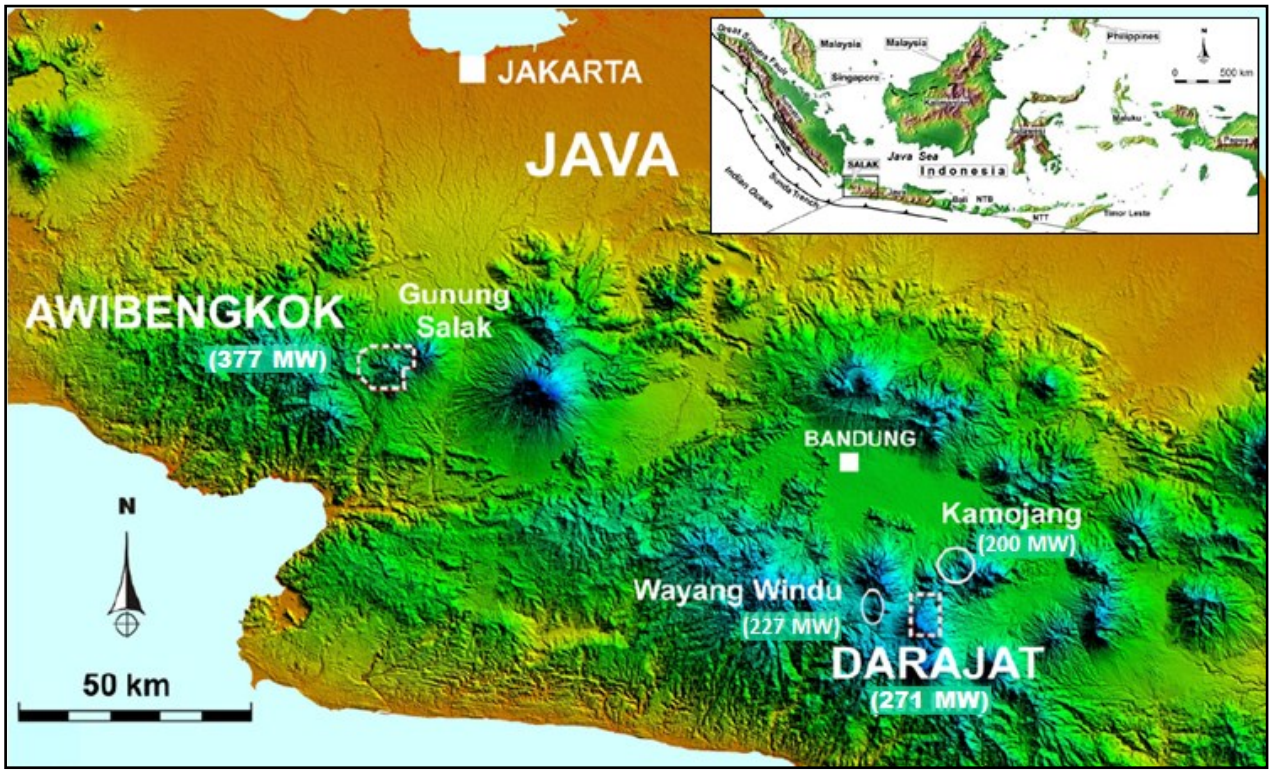

Figure 1: Map of West Java showing major cities and volcanic centers. Also shown are the Awibengkok/Salak and Darajat geothermal contract areas (dashed polygons) and other producing geothermal fields in the general area.

Salak is a liquid-dominated geothermal system with a moderate- to high-temperature (464°-600°F) fracture-controlled reservoir hosting benign and low to moderate non-condensable gas (NCG) fluids. The geothermal reservoir is associated with young volcanism and intrusions in a highland area west of Gunung Salak and east of the Cianten caldera, a collapsed andesitic stratocone. The youngest volcanic vents are concentrated along a NNE-trending Awi and Cibeureum faults. Predominant fault and fracture orientations are N-to-NE, with subsidiary NW and E-W trends. Based on unpublished K–Ar and $^{40}Ar/^{39}Ar$ dating, the major peaks of the Salak area were built from 860 to 180 ka, whereas the ancestral andesitic cone that forms the rim of the Cianten Caldera to the west was active from about 1610 to 670 ka (**Figure 2**). Within the Salak production area, andesitic to rhyodacitic tuffs and lavas dated from 185 to 280 ka and are overlain by rhyolitic domes, lavas and related tephra sequences which were erupted primarily along a NNE-trending fault that crosses the eastern portion of the field. The age of this rhyolitic volcanism is from 120 to 40 ka based on K–Ar and $^{40}Ar/^{39}Ar$ dating. The uppermost silicic unit is an extensive tephra known as the "Orange Tuff". The age of this unit is bracketed between 40,000 and 8400 years B.P. by ^{14}C dates on underlying lahar and overlying hydrothermal breccia units (Stimac et al., 2008).

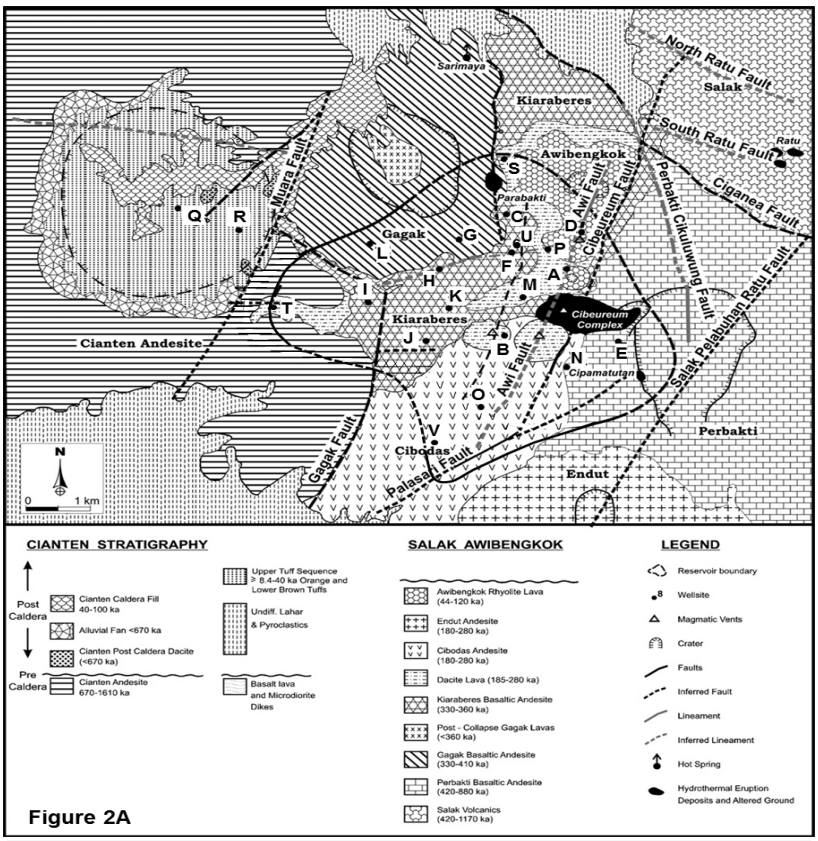

Figure 2A

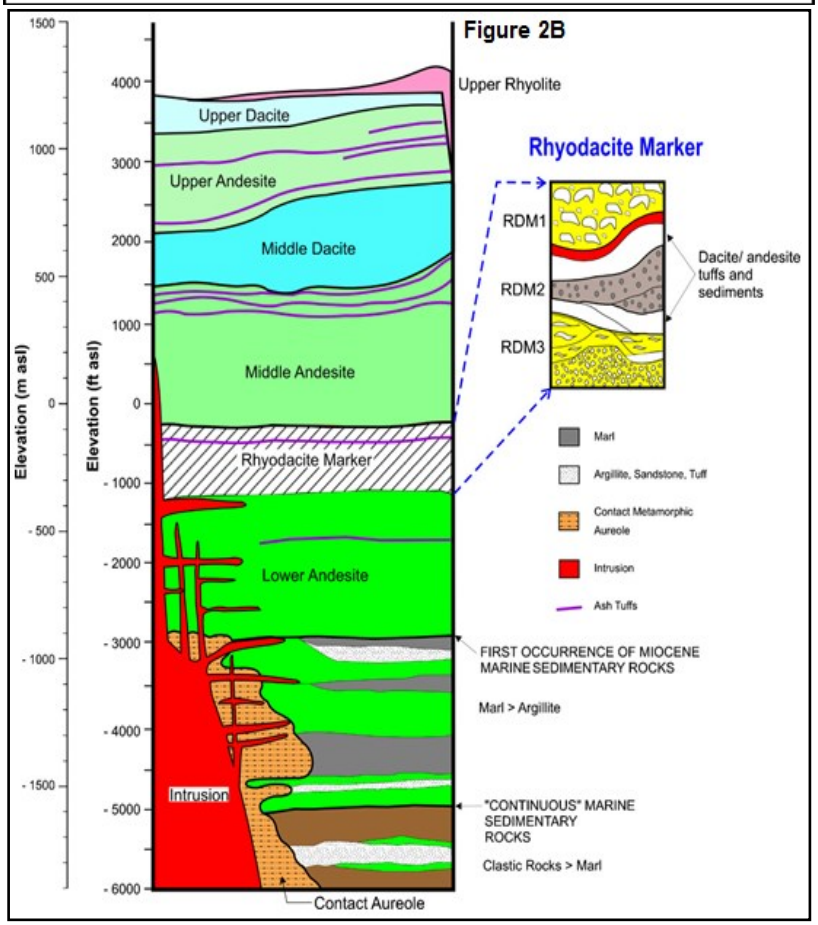

Figure 2: (2A) Surface geology of the Salak area showing major rock types, prominent faults, altered ground, current reservoir boundary and well Pad locations. Also shown is the Sarimaya chloride spring for reference. Ages are shown in thousands of years (ka). This map was modified from Stimac et al. (2008). (2B) Representative stratigraphic column for the Awibengkok reservoir.

The reservoir is contained primarily within a sequence of volcanic rocks of andesitic to rhyodacitic composition with a basement of Miocene marine sedimentary rocks. Both volcanic and sedimentary rocks are cut by igneous intrusions (Stimac et al., 2008). The stratigraphic section can be divided into four major formations thought to represent discrete episodes in the evolution of the western Java segment of the Sunda Volcanic Arc. These are: (1) Shallow-Marine Carbonates and Epiclastic Sediments (mudstones and sandstones containing abundant volcanic ash and lithic debris); (2) Lower Volcanic Formation, consists of andesitic to basaltic volcanic rocks, overlies and is interbedded with the upper Miocene sedimentary section; (3) Middle Volcanic Formation, which is another sequence of andesitic-to-dacitic lavas, tuffs, lahars, and debris flows that represents construction, collapse and erosion of stratovolcanoes and lava dome complexes. In this formation, there is widespread rock that represents an episode of silicic volcanism and caldera formation that followed the first major episode of andesitic stratovolcano construction in the area, namely Rhyodacite Marker; and (4) Upper Volcanic Formation consists of another andesitic sequence overlain by dacitic to rhyolitic rocks that includes the surface deposits described above. Each major volcanic formation is further subdivided into a lower andesitic section and an overlying rhyolitic or dacitic section. These formations are inferred to represent distinct or partially overlapping volcanic episodes that each evolved to become more silicic with time (**Figure 2**).

3. 3D GEOLOGIC MODEL

The Salak 3D geologic models have been constructed for various purposes including: (1) a tool to integrate all available geological, petrophysical, geophysical, geochemical and reservoir engineering information to better understand the geothermal system; (2) providing geologically sound input for numerical modeling; (3) for well planning; and (4) for development of reservoir characterization and modeling proficiency within the organization. Earth modeling is an iterative process and is focused towards developing efficient and re-usable workflows and generally away from the resulting "pile" of geocells. For the Salak 3D Earth modeling work, an evergreen static modeling workflow was built in Chevron's in-house 3D modeling software. This workflow allows the modelers to easily update the static model whenever new input data is acquired.

Copious subsurface data was acquired during the series of make-up drilling campaigns in Salak. Thirteen new wells were drilled in various locations around the field in the recent 2012-2013 drilling campaign. Various types of data (reservoir geology, geochemistry, geophysics, drilling, reservoir engineering, and field performance) had been accumulated since 2008 which encouraged the Salak 3D modeling team to update the previous earth model. A robust geothermal system earth model comes from the integration of both subsurface and surface data.

3.1 Geologic Structures

The Salak 3D earth modeling team identified several lineaments and structures that control fluid flow, distribution of permeable entries, offsets in lithologies and other reservoir characteristics (e.g., pressure differences between reservoir cells, tracer flow pathways, alignment of micro-earthquakes (MEQs), etc.). **Table 1** shows the categorization of the mapped lineaments and faults in Salak based on their impact to the geothermal reservoir and level of confidence (regarding their physical presence). **Figure 3** shows the mapped faults and lineaments identified at Salak with the different colors representing the levels of impact to geothermal system and confidence on their physical evidence.

Fault/ Lineament	Physical Evidence					Impact To Geothermal System			
	Offset Lithology (RDM)	Geophysics (MEQ)	Image Log	Surface Expression	Level of Confidence	Large Scale fluid flow impact	Alignment of Entries	Reservoir Eng. Data	Level of Impact to Geothermal System
East Cisaketi	√	None	√	√	High	√	√	None	High
Awibengkok	√	√	√	√	High	√	√	None	High
Cibereum	√	None	√	√	High	√	√	√	High
MEQ1	√	√	√	√	High	√	√	None	High
MEQ2	√	√	√	√	High	√	√	None	High
NW-I8	None	None	√	√	High	√	√	None	High
Cibodas	√	None	None	√	Medium	√	√	None	High
NW-D1	None	√	None	√	Medium	√	None	None	High
Muara	√	√	√	√	High	√	None	None	Medium
Palasari	√	√	√	None	High	√	None	None	Medium
Gagak NW	None	None	√	√	Medium	None	√	√	Medium
Gagak NE	None	None	√	√	Medium	√	None	None	Medium
Gagak	√	None	N/A	√	Medium	√	None	None	Medium
Sarimaya	None	√	√	√	Medium	√	None	None	Medium
SPR	√	None	N/A	None	Medium	√	None	None	Medium
Parabakti	√	None	N/A	√	Medium	√	None	None	Medium
Gareok	√	√	√	√	High	None	None	None	Low
Caldera Ring	√	√	None	√	High	None	None	None	Low
West Cisaketi	None	√	N/A	√	Medium	None	None	None	Low
Cianten	√	None	N/A	√	Medium	None	None	None	Low
Pangguyangan	√	None	N/A	√	Medium	None	None	None	Low
Ciasmara	None	None	N/A	√	Low	None	None	None	Low
Ratu North	None	None	N/A	√	Low	None	None	None	Low
Ciganea	None	None	N/A	√	Low	None	None	None	Low
Ratu South	None	None	N/A	√	Low	None	None	None	Low

Table 1. Summary of mapped faults and lineaments in Salak

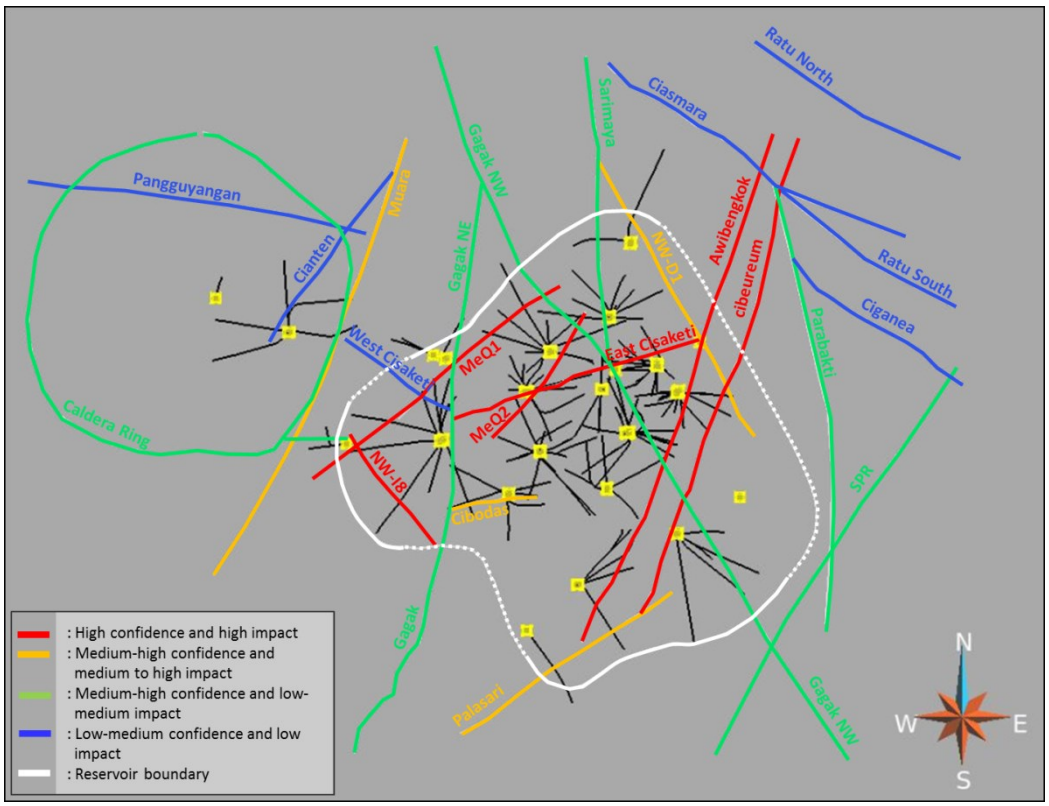

Figure 3: Map showing the mapped faults and lineaments in Salak. Each color represents the degree of confidence (of the structure's presence) and impact of the particular structure to the Salak geothermal system.

3.2. Lithology

The reservoir rocks at Salak are composed mainly of andesitic and lesser basaltic lava flows, breccia, tuff and lahar that comprise several long-lived volcanic centers underlying the southwestern margin of Gunung Salak (Hulen et al., 2000; Stimac and Sugiaman, 2000). Thick rhyodacitic to dacitic ash-flow tuffs and associated domes, breccias and lahars are interspersed with the more voluminous andesitic to basaltic sequences that date back to Miocene times (Stimac et al., 2008).

The subsurface lithology modeling was inferred from descriptions of drill cuttings and supplemented by spot cores from 16 wells and 1,067 meters of continuous core from one production well in east Salak. Borehole resistivity images and gamma-ray logs also provided constraints on major rock types and compositions, respectively, and are the only means of obtaining lithologic] data in the reservoir hole sections of wells which were drilled without mud returns. This data was used as basis for the 3D representation of the subsurface litholigies and intrusive bodies in the static model **(Figure 4).**

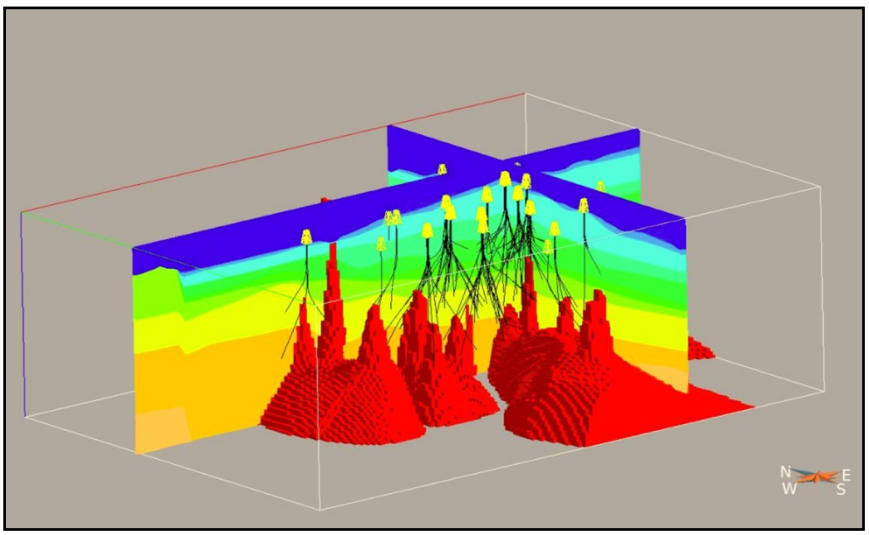

Figure 4: Screenshot showing the distribution of subsurface lithology in the Salak 3D Earth Model. The red blocks represent the intrusive bodies as encountered with the drilling and their possible distribution beneath the drilled depths.

3.3. Hydrothermal Alteration

The distribution of hydrothermal alteration play important role in determining the reservoir extent and petrophysical properties distribution. Hydrothermal alteration zones in Salak were identified mainly from rock cuttings and core. Magneto-Telluric (MT) resistivity data was used as a constraint for the distribution of clay alteration at the periphery of and outside the reservoir area. In general, hydrothermal alteration in Salak can be categorized into three main zones, namely, argillic, transitional argillic-propylitic, and propylitic. Phyllic alteration was also identified in some wells but its distribution is not extensive; our current interpretation is that phyllic alteration in Salak is highly correlated with the presence of silicic rocks. Furthermore, the petrophysical measurements (i.e., matrix porosity, matrix permeability) acquired from the propylitic and phyllic zones do not show significant differences. Therefore, in the current Salak 3D earth model surfaces that define the boundaries of argillic, transitional argillic-propylitic, and propylitic alteration are represented as continuous and widespread, while phyllic alteration is localized in small pockets.

Argillic alteration is dominated by smectite clay, with accessory pyrite, hematite, calcite, anhydrite and zeolites that formed at temperatures less than about 180°C. The rocks within this alteration zone typically have resistivity below about 10 ohm-m and a conductive temperature profile indicating very low fracture permeability. The argillic alteration has been successfully mapped with methylene blue (especially during drilling) and X-ray diffraction analyses of cuttings in selected wells. The transitional argillic-propylitic zone can span up to 300 m in thickness, and is dominated by mixed layered smectite–illite clay with chlorite, calcite, pyrite, titanite and quartz. The propylitic alteration zone is dominated by chlorite, epidote, illite and quartz, but also contains albite, adularia, calcite, wairakite, pyrite, anhydrite and titanite. This alteration assemblage corresponds to measured reservoir temperatures between about 220 and 270 °C.

Figure 5 shows a cross-section of the hydrothermal alteration at Salak in the 3D earth model. The argillic and transitional argillic-propylitic zones extend to the west of Salak reservoir (Cianten caldera), as do the low resistivities measured by MT. However, the temperatures beneath the clay cap in Cianten are significantly lower compared to Salak indicating cooling has taken place (Nordquist, 2007). It is believed that there was once an active geothermal system within the Cianten caldera that has since collapsed. We have taken the top of the propylitic alteration assemblage to be the "most likely" top of reservoir.

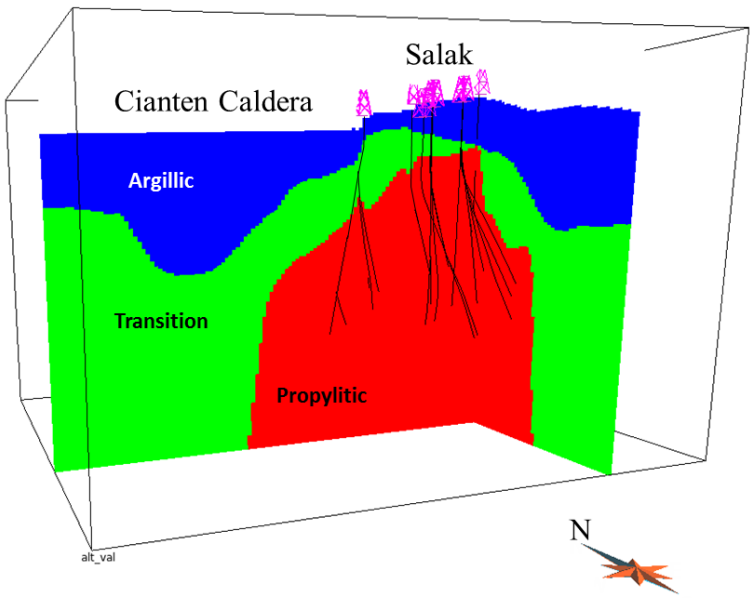

Figure 5: Screenshot showing the hydrothermal alteration at Salak in the 3D Earth Model. Although the argillic alteration extends to the west, this alteration assemblage is believed to have been associated with the earlier active geothermal system under the Cianten caldera.

3.4. Temperature Distribution

As a key parameter in reservoir characterization, the initial or pre-exploitation temperature was integrated into the 3D earth model. The main objective in building a 3D representation of initial temperatures is to enable querying of commercial reservoir volume for uncertainty analysis and development of a workflow that will allow use of simple parameters to easily update the 3D model whenever new data is acquired.

The temperature profile of a typical Salak well has three main regions - conductive, transition from conductive to convective and isothermal (**Figure 6**). Three regions were constrained using six variables, namely, Z_0, T_0, Z_1, T_1, Z_2 and T_2. Z_0 and T_0 represent the elevation of the well and temperature at surface, respectively. The elevation and temperature of the top of the transition from conductive to convective region are denoted by Z_1 and T_1, while Z_2 and T_2 indicate top of isothermal zone elevation and temperature.

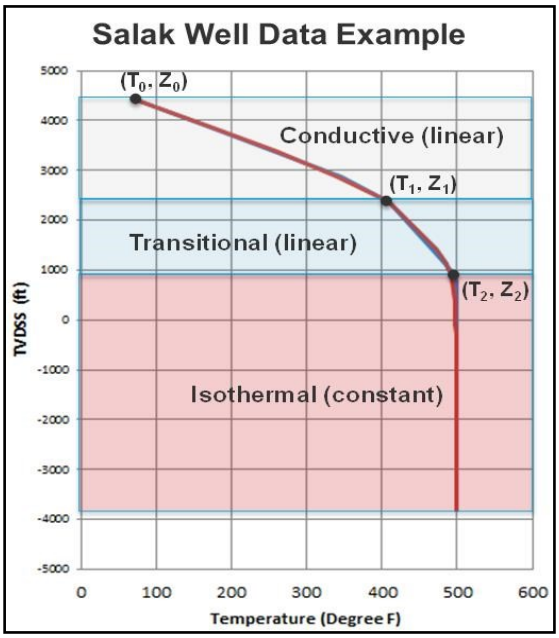

Figure 6: Schematic showing the temperature profile parameterization of a typical Salak well.

The above six variables from each well temperature profile were interpolated into the "surfaces" in the 3D model. The interpolated values were vertically projected into the grid using linear vertical interpolation (**Figure 7**). A regional temperature profile was applied outside of the reservoir and used as a lower limit within the reservoir area.

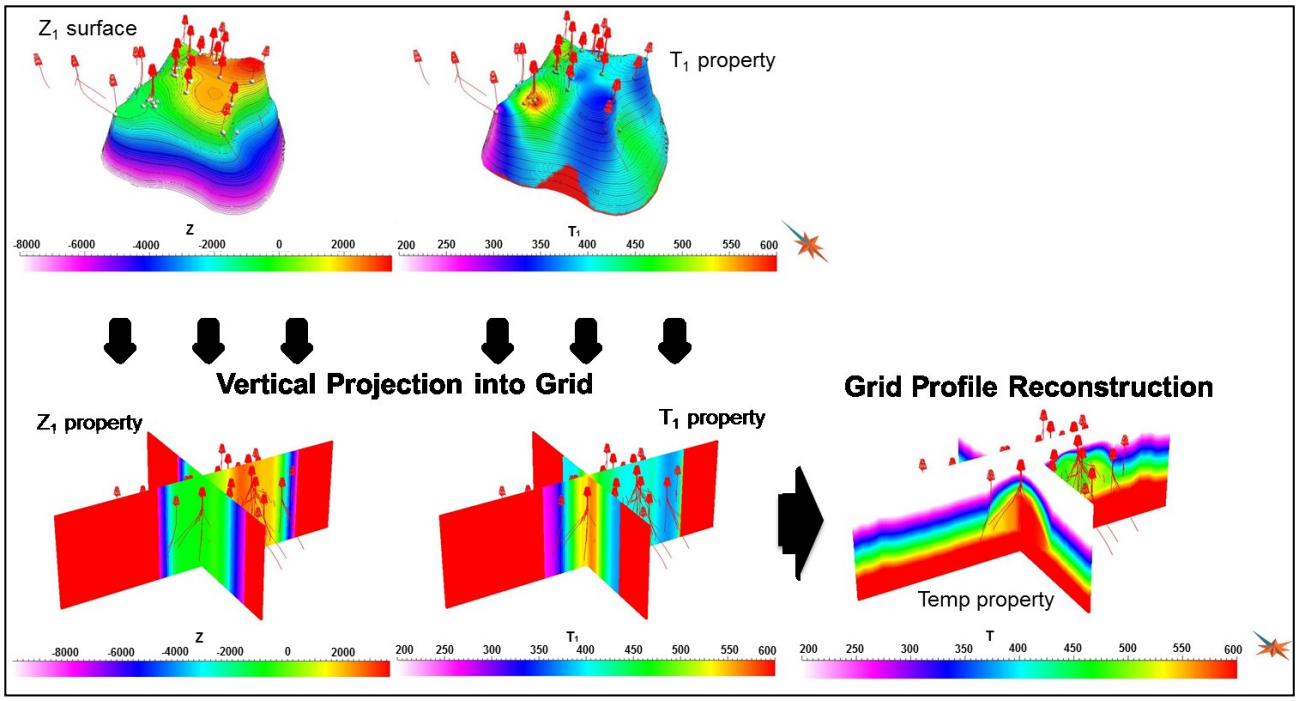

Figure 7: Schematic showing the temperature modeling workflow.

Figure 8 is a cross-section showing the temperature profile from SW to NE, as derived from the 3D earth model. The initial temperature distribution characterizes both permeability and heat flow in the geothermal system. The upflow of the Salak geothermal system is located in the western portion of the field (Pad I area) where the highest temperatures have been measured. The hot fluid ascends buoyantly from the deep upflow and moves in two preferential directions, to the northeast towards Pad C and Parabakti fumarole, and also to the southeast towards Pad O, possibly to the south of Pad N, or below the Cipamatutan fumarole. Thermal discontinuities allow the field to be subdivided into distinct sectors or "cells" that are likely bounded by faults, which are shown as an abrupt temperature change in Figure 9. The most common cause for such discontinuities in thermal regimes is a sharp change in permeability.

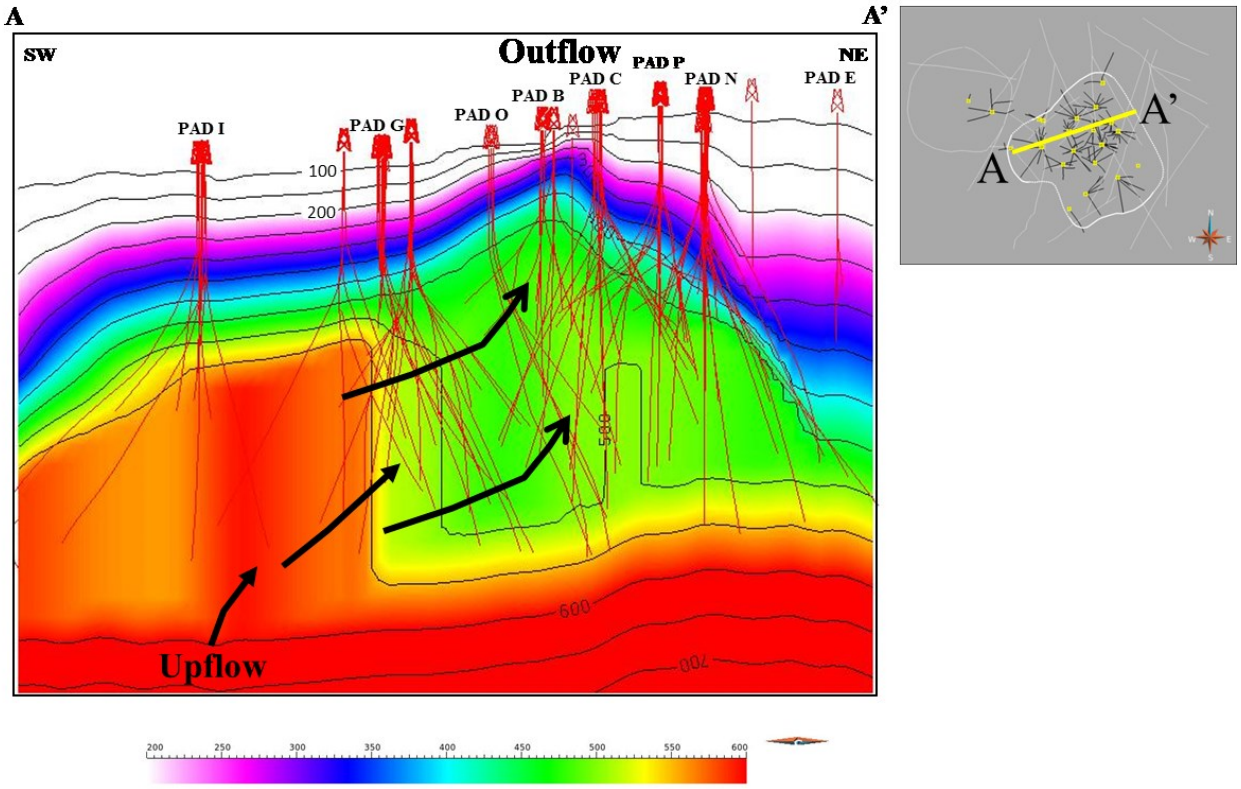

Figure 8: Cross-section from the 3D Salak Earth Model showing the temperature (in °F) profile from SW to NE.

3.5. Reservoir Top and Base

Table 2 summarizes the criteria used to define the top and base of the Salak geothermal reservoir. In this work, the parameters used to define the top of reservoir are similar with what was used in the previous model in the mid-2000; hence the top of reservoir did not change significantly with the addition of the new data. The base of the geothermal reservoir was defined as the maximum depth at which the fracture permeability of the rock is high enough to sustain commercial flow. Aprilina and Golla (2012) defined this to correspond more or less to a fracture permeability of around 1 – 5 mD. In the current 3D model, the deepest well entries were used as basis for our estimate of the shallowest (P10) base of reservoir. The most likely (P50) and deepest (P90) base of reservoir estimates were made based on qualitative and interpretative mapping of MEQ densities below drilled reservoir depths. The P50 and P90 bases of reservoir estimates used MEQ density criteria of 0.5 and 0.1 hypocenters per 250 x 250 x 250 m block), respectively. These MEQ density surfaces were liberally smoothed due to lack of MEQs in certain areas of the reservoir.

Based on the results of the 2012-2013 drilled wells, the deepest reservoir bottom is located in the southwestern portion of the Salak field where the upflow is located. The deepest entry at -6,286' elevation (-1,916 m) was encountered by a recently drilled well during the 2012-2013 Salak drilling campaign. MEQ hypocenters indicate that permeability could extend as deep as -13,000' (-3,963 m) elevation in this part of the field. There are geothermal reservoirs where substantial reserves have been found below a previously interpreted reservoir bottom (e.g. Larderello, Italy; Mak-Ban, Philippines) hence a "very" deep well may be drilled to reduce the uncertainty in this regard.

Top of Reservoir Criteria

Criteria	Top of Reservoir		
	Low	Mid	High
Drilled Region			
Entry	x		
Continuous Epidote	x	x	
Convective Profile	x	x	x
Temperature (deg F)	> 460	> 450	>425
First Epidote			x
Undrilled Region			
Wells	Include	1000 ft out	2000 ft out
Fumaroles	Include		1000 ft out
Faults		x	
MT/TDEM			x

Base of Reservoir Criteria

Reservoir Base		
Low	Mid	High
The deepest entries encountered by deepest well plus 150m	Interpretation of distribution of MeQ hypocenters (0.5 as cut off)	Interpretation of distribution of MeQ hypocenters (0.1 as cut off)

Table 2. Criteria used to define the top and base of the Salak reservoir

3.6. Rock Properties

For the purpose of earth model construction, the reservoir rocks in Salak are grouped into six petrophysical groups (PG). The petrophysical grouping was aimed at simplifying the different lithologic units to a level that can be justified with reasonable confidence by considering the contrast mainly in the petrophysical properties, depositional styles and hydrothermal alteration. This grouping was done to reduce complexity or optimize computing time as less model components mean faster computing time. From about nine different lithologies identified, six rock groups were determined, namely, PG1 (metamorphic rocks or skarn; lowest matrix porosity), PG2 (sedimentary rocks, i.e., argillite, mudstone and limestone), PG3 (crystalline intrusives such as dacite, granodiorites and diorite/microdiorite), PG4 (andesitic-dacitic lava flows), PG5 (fine-grained tuff and lithic tuff) and PG6 (coarse-grained pyroclastic like breccias, ash-flow tuff and lahar). **Table 3** shows the global facies proportion of these PGs in each stratigraphic unit (formation) which were used in the PG populating.

Formation	PG Average in Each Formation					
	PG1	PG2	PG3	PG4	PG5	PG6
UD	0	0.00601202	0	0.182365	0.691383	0.12024
UA	0	0.00263435	0	0.352213	0.566122	0.0790306
MD	0	0.00313245	0.000272387	0.383997	0.423085	0.189513
MA	0	0.00231911	0.000154607	0.223871	0.607143	0.166512
RDM	0	0.00247666	0.000190512	0.334826	0.431416	0.231092
LA	0	0.00933748	0.0146732	0.181859	0.771009	0.0231214
MVS	0	0.0106045	0.0166136	0.392365	0.472959	0.107458
CS	0.0194907	0.199937	0.236089	0.238604	0.22603	0.0798491
INT	0.0021978	0.186813	0.345055	0.0901099	0.327473	0.0483516

PG1 : skarn
PG2 : sediments
PG3 : intrusion
PG4 : lava
PG5 : fine grain pyroclastics
PG6 : coarse grain pyroclastics

Table 3. Global facies proportion of six PG in each stratigraphic unit (formation)

The six PG facies were populated in the 3D earth model using Indicator Kriging and Sequential Indicator Simulation. The populated probabilities and realizations honor the local facies at the well, and global facies proportions calculated within each stratigraphic unit. **Figure 9** shows the PG facies population in new Salak 3D earth model.

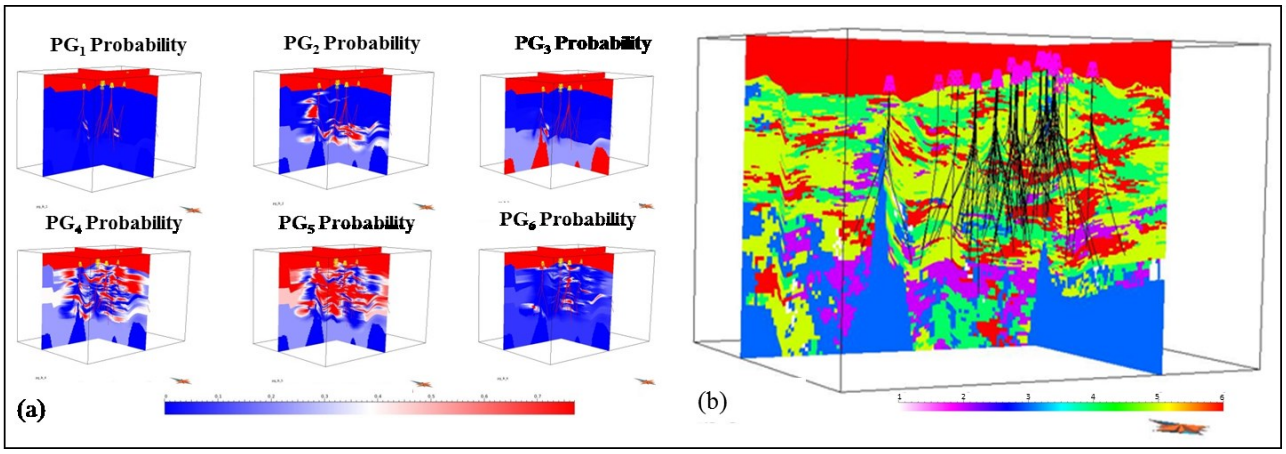

Figure 9: Screenshots showing the PG facies distribution in the 3D Earth Model. The six PGs were distributed using Indicator Kriging (a) and Sequential Indicator Simulation (b).

3.6.1. Matrix Porosity

The matrix porosity data were taken from both conventional and sidewall core plugs with helium porosity measurements. **Figure 10** shows the summary of matrix porosity for each PG.

Series Name	Average Matrix Porosity (%)	Number of Samples
PG1	0.92	12
PG2	3.32	24
PG3	3.71	11
PG4	6.45	44
PG5	8.53	52
PG6	12.06	57

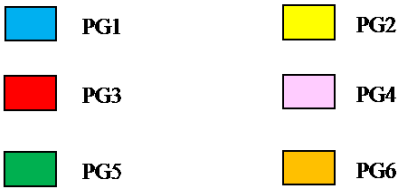

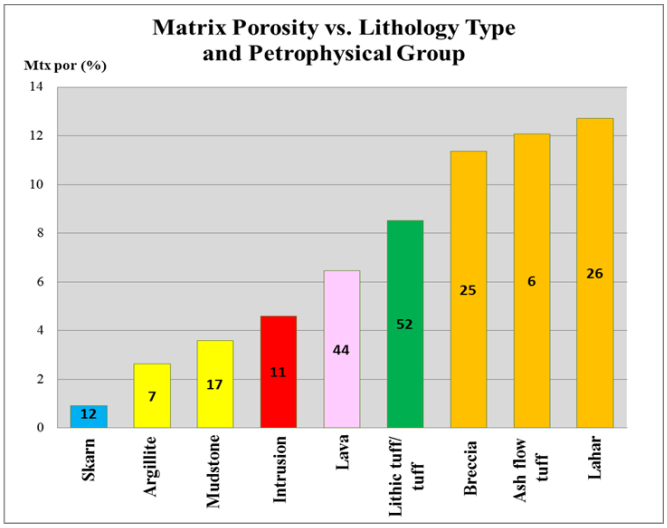

Figure 10: Charts showing the summary of matrix porosity for each PG in Salak. The fine-grained sedimentary and metamorphic rocks have the lowest matrix porosity while the coarse-grained pyroclastics (i.e., breccias, ash-flow tuff and lahar) have the highest matrix porosity. The average matrix porosity of the lava flows, which comprise majority of the Salak reservoir, is about 4 – 6 %.

Based on regression analysis, the matrix porosity shows a statistically significant correlation with alteration type, facies and elevation. The depth-related trend for rocks inside the reservoir is linked with the zonation of hydrothermal alteration. Reservoir rocks with propylitic alteration appear to have enhanced matrix porosity indicating that the dominant process during alteration is dissolution (rather than deposition) of minerals. This observation is also true and was observed at both Tiwi and Darajat (Powell, T.S, 1996; Fitriyanto et al., 2012). Outside (or above) the reservoir, hydrothermal alteration doesn't have significant influence on matrix porosity. In the 3D Earth Model, matrix porosity was distributed laterally using Indicator Kriging of PG (**Figure 11**). To populate matrix porosity vertically, regression weights for rocks inside and outside the reservoir were applied using Equation 1 below:

$$\text{Matrix Porosity} = a*Z + b*P(PG1) + c*P(PG2) + d*P(PG3) + e*P(PG4) + f*P(PG5) + g*P(PG6) \quad \text{(Equation 1)}$$

Where: Z is depth in feet elevation;
P(PG#) is PG indicator probability; and
a, b, c, d, e, f, and g are linear regression weights.

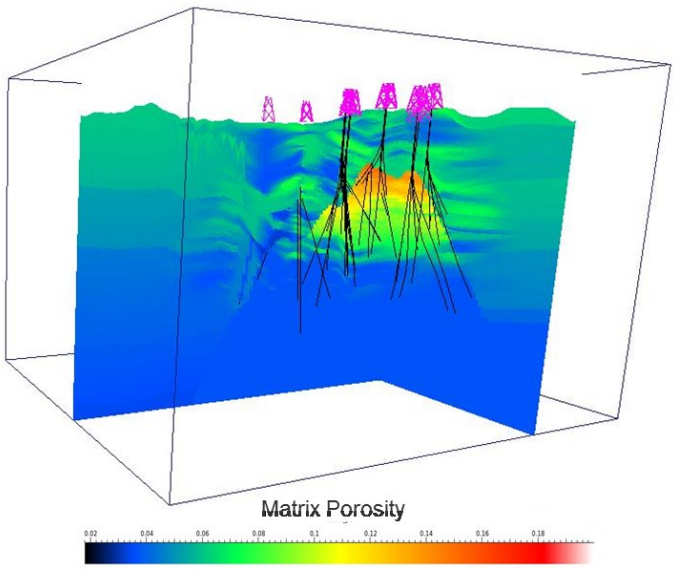

Figure 11: Screenshot showing matrix porosity distribution in the Salak 3D Earth Model.

3.6.2. Matrix Permeability

The matrix permeability data were taken from the same core plugs of the matrix porosity samples. **Figure 12** shows the summary of matrix porosity for every PG. Unlike matrix porosity, only the zonation of hydrothermal alteration has statistical significance with regards to the matrix permeability. Rocks located in the clay cap zone, where the smectite clay mineral is abundant, tend to have lower matrix permeability, probably because clay fills previous open space in the matrix. Therefore in the 3D earth model, matrix permeability was populated in three different regions, i.e., inside the reservoir, outside (or above) the reservoir, and in the clay cap zone (**Figure 13**).

Series Name	Inside Reservoir		Outside Reservoir		Clay Cap	
	Average Matrix Permeability	Number of Sample	Average Matrix Permeability	Number of Sample	Average Matrix Permeability	Number of Sample
PG1	0.04	1	0.08	9	-	0
PG2	0.44	8	0.17	15	-	0
PG3	0.01	3	0.01	5	-	0
PG4	0.07	34	0.01	9	0.01	2
PG5	0.06	31	0.08	16	0.01	2
PG6	0.19	35	0.01	5	0.03	17

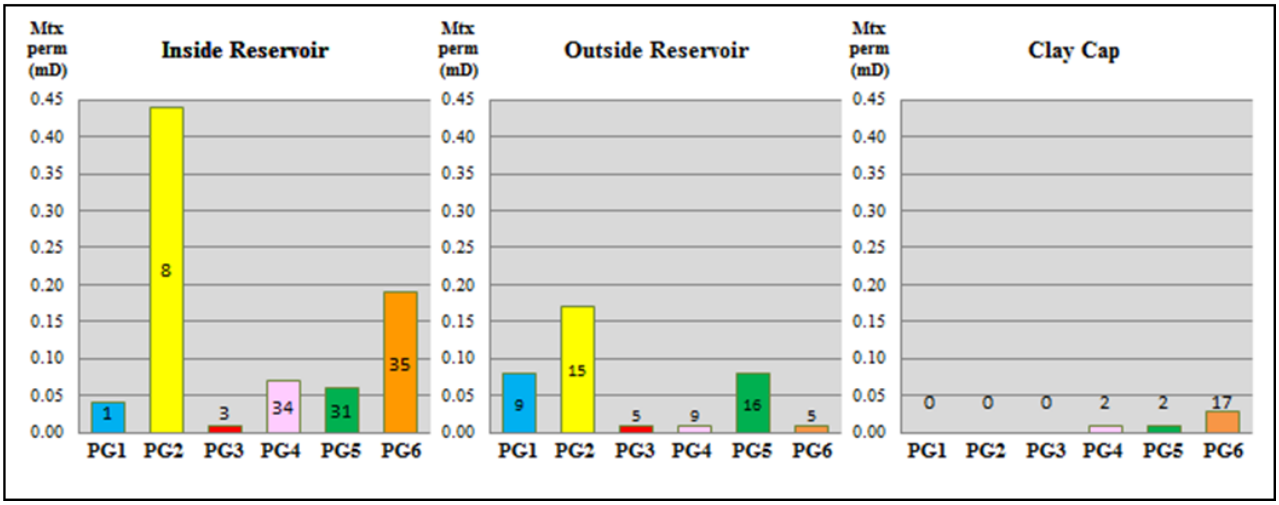

Figure 12: Charts showing the distribution of matrix permeability for each PG and inside, outside and within the clay cap of the Salak reservoir.

Matrix permeability was distributed based on PG rock type probabilities (Indicator Kriging) using the mean of PGs for each region with below equation:

Matrix Permeability = a*P(PG1)+b*P(PG2)+c*P(PG3)+d*P(PG4)+e*P(PG5)+f*P(PG6) (Equation 2)

Where: P(PG#) is PG indicator probability; and
a, b, c, d, e, f, and g are linear regression weights.

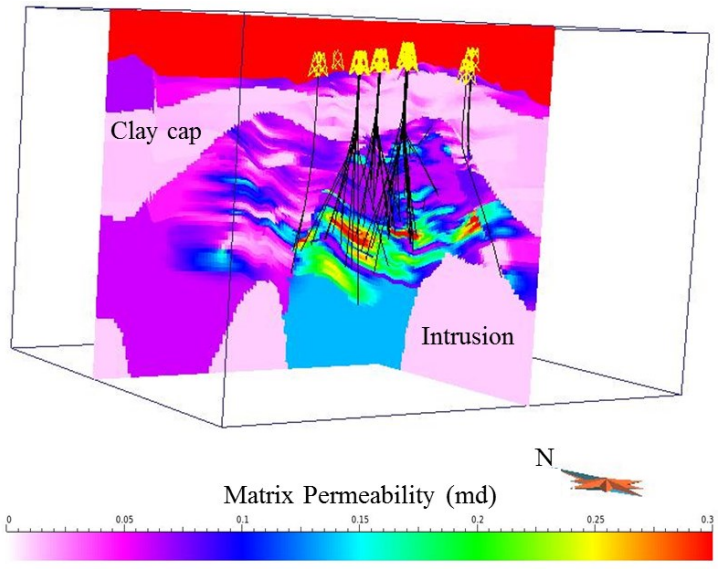

Figure 13: Screenshot showing matrix permeability distribution in the 3D Earth Model.

3.7. Commercial Reservoir Volume

As the geological and geophysical constraints do not uniquely prove any single geologic model for the field, low (P10), mid (P50) and high (P90) exploitable resource extent are defined. In a conventional 3D model, the top, bottom, and lateral extent of the commercial reservoir are usually described as a non-discrete surface. A new approach in defining the commercial reservoir volume is being applied in the current Salak 3D model. Model properties are queried using criteria to define different volume realizations. The workflow used in the volume realizations allows automated modification in particular realization (not only restricted to

low/P10, mid/P50, and high/P90) by modifying the queried criteria. **Figure 14** shows three probabilistic reservoir volume realizations using the low (P10), mid (P50) and high (P90) tops and bases of reservoir.

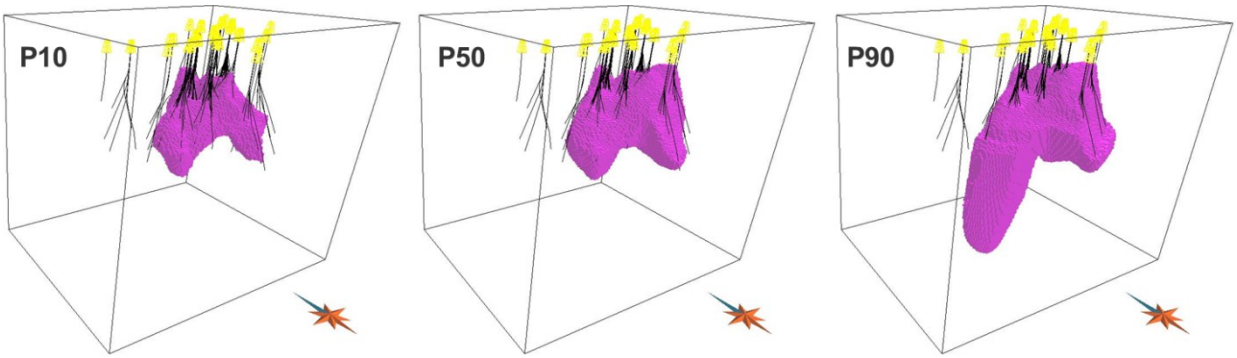

Figure 14: Screenshot showing the three probabilistic volume realizations using the P10, P50 and P90 tops and bases of reservoir.

4. SUMMARY

An iterative multidisciplinary (geology, geophysics, geochemistry and reservoir engineering) approach can better represent the conceptual model of a geothermal system into a 3D earth model. The process of reconciling and integrating such a diverse set of inputs helps in building common team understanding and alignment. The earth model is an evergreen tool that can be updated periodically with data from recently drilled wells and new reservoir performance data, hence the importance of documenting modeling steps or approaches and workflows.

The conceptual model of the Salak geothermal system has been realized in a 3D digital model by applying a geostatistical modeling approach to provide a better representation of reservoir properties. Eventually, this 3D earth model will be used as basis for a numerical simulation model which will aim to predict reservoir performance and support field management decisions such as injection management and make-up well targeting.

During the 2012-2013 drilling campaign, this 3D earth model was used for well trajectory planning and design. The model provided a better representation of drilling targets such as fractures and specific formations. It was also very useful in viewing real time trajectories as the wells were being drilled, avoiding potential collisions and production interference with offset wells.

5. ACKNOWLEDGEMENT

The authors would like to acknowledge the contribution of all Salak Asset Management Team and Chevron Geothermal Indonesia, Ltd. colleagues in this 3D modeling work and Chevron IndoAsia Business Unit management for the permission to publish this paper.

REFERENCES

Aprilina, N.V. and Golla, G.: Salak Interim 3D Static Model Update, *Chevron Geothermal Indonesia Internal Report* (2012).

Baroek, M.C., Aprilina, N.V., Sunio, E., Nelson, C., Peter: North Awibengkok Subsurface Evaluation, *Chevron Geothermal Indonesia Internal Report,* 46 pp, Mar 4, 2011.

Day, P.I.: Log Analysis of Awibengkok 1-2 and Awibengkok 1-2ST, *Unocal Geothermal Indonesia Internal Report* (1996).

Fitriyanto, Agus, Intani, R., Mahagyo, P., Golla, G. and Waite, M.: The 2012 Darajat 3D Static Model: General Workflows and Steps to Build a 3D Static Model, *Chevron Geothermal Indonesia Internal Report,* 40 pp, June 7, 2012.

Nordquist, G.: Re-interpretation of Cianten Caldera Geophysical data using constraints from Awi 17 and 18, *Chevron Geothermal Indonesia Internal Report* (2007).

Powell, T.S.: Matrix Porosity and Permeability of the Matalibong-25 Core, *Unocal Geothermal Philippines Internal Report* (1996).

Powell, T.S.: Matalibong-25 Porosity Studies Update, *Unocal Geothermal Philippines Internal Report* (1997).

Rohrs, D.: AWI1-2 Core: Lithology and Porosity Distributions, *Unocal Geothermal Philippines Internal Report* (1996).

Rohrs, D., Gunderson, R., Melosh, G., Suminar, A., Nordquist, G., Molling, P., Sirad-Azwar, L. and Acuna, J.: Awibengkok 2005 Conceptual Model Update, *Chevron Geothermal Indonesia Internal Report* (2005).

Stimac, J., Astra, D., Molling, P., Acuna, J., Prabowo, H. and Sugiaman, F.: Awibengkok 1997 Conceptual Model Summary, *Chevron Geothermal Indonesia Internal Report* (1997).

Stimac, J., Nordquist, G., Suminar, A. and Sirad-Azwar, L.: An Overview of the Awibengkok Geothermal System, Indonesia, *Geothermics*, **37** (2008), pp 300-331.

Stimac, J., Baroek M.C.: AWI1-2 Core Analysis Report*, Chevron Geothermal Indonesia Internal Report* (2010).

Soeparjadi, R., Horton, G.D., Bradley, E., Wendt, P.E.: A review of the Gunung Salak Geothermal Expansion Project, *Proceedings,* 20th New Zealand Geothermal Workshop, Auckland (1998), pp. 153–158.